



Wind Loads on Heliostats and Photovoltaic Trackers

Shaik Nayabu Rasool^a, M.Mahesh^b

^aPG Student, Guntur Engineering College, Department of Mechanical Engineering, Guntur, AP, India

^bAssociate Professor, Guntur Engineering College, Department of Mechanical Engineering, Guntur, AP, India

ABSTRACT

For a cost-effective design and dimensioning of heliostats and photovoltaic trackers the wind loading must be known as precisely as possible. Properties of the heliostat itself like size, aspect ratio, gaps in the mirror panel, and the kind of stow position are of impact on the wind loads as well as other parameters of the heliostat field like wind fence, heliostat field density, and position within the field. By atmospheric boundary layer wind tunnel investigations these impacts are determined. In the wind tunnel the wind conditions at full scale must be matched. The highest Reynolds numbers and larger eddies cannot be reproduced by usual boundary layer wind tunnels. It is investigated whether these deficits can be neglected for the investigation of heliostats and PV trackers. Also, the maximum gust duration has an impact on the wind loading. By full scale measurements it is investigated whether the maximum gust duration is limited enough that the maximum loads could be reduced by shock absorbers. The theory of extreme value statistics for the determination of the wind load peak values and the correlation between eddy diameters and turbulent energy spectra are explained in the appendix.

Keywords: Photovoltaic Trackers, Heliostats, Photovoltaic Trackers

1. Introduction

In a solar power plant, temperatures up to 700° C are reached by moving mirror systems called "heliostats" tracking the sun and concentrating its radiation to the top of a tower for large scale electricity production and industrial process heating. To enable a breakthrough of this solar energy technology the heliostat costs have to be further reduced. With precise knowledge of the wind loads they can be built lighter and cheaper. The objective of the presented thesis is to close knowledge gaps and to reduce uncertainties regarding the wind ...

1.1 Solar Tower Plants

Concentrated solar thermal (CST) energy is a promising renewable energy technology capable of large-scale electricity production and industrial process heating, usually incorporating energy storage. The main CST technologies are dish-Stirling systems, linear Fresnel systems, trough systems and tower systems. In a solar tower plant, moving mirrors called 'heliostats' track the sun in two axes and reflect the sun's rays onto a 'receiver' at the top of a tower (Fig. 1).



Fig. 1

The receiver absorbs the radiation and supplies thermal energy via a working fluid at a temperature of typically 300-700°C. At solar power plants the thermal energy is converted into electrical energy which is then called concentrated solar power (CSP). For power towers incorporating energy storage, the working fluid is usually also a heat storage medium (e.g. molten salt), and is stored in tanks to allow power generation upon demand. Alternatively, the energy received by the solar towerplant may be used for providing heat to a thermochemical process, such as the production of synthetic transport fuels.

A photovoltaic (PV) power plant currently provides electrical energy at a lower cost than a CSP plant. However, storage of electrical energy is in general more expensive than storage of thermal energy. Therefore, PV plants that would require electrical energy storage are more suitable for power supply during sun hours and CSP plants during the night and in cloudy conditions because they can use less expensive thermal energy storage. A combination of both PV and CSP is seen as a promising solution for future power supply: “The cost of solar technologies are falling so quickly that within a few years the combination of solar PV and solar towers with storage will be able to compete directly with base load fossil fuels” (Padmanathan, 2015). Indeed, this aim was reached in 2017 by several bidding prices (see e.g. (Clean Technica, 2017)). An important advantage of CSP compared with PV is that during construction a high fraction of labour and equipment is sourced locally, which is especially attractive for developing countries.

Examples of industrial processes that could be driven by solar tower plants are cement production (González and Flamant, 2014) and enhanced oil recovery (CSP today, 2013). Solar tower systems can also supply competitively heat to thermal processes at 550°C or below, although 500°C has been achieved as well by some small CSP demonstration plants with trough collectors which had been of lower cost so far. Many industrial processes are designed for higher working temperatures, which are provided by fossil fuel burners. To incorporate solar input, it is sufficient to replace only the burner with a solar receiver and the rest of the plant stays almost unchanged. With further reduction of the cost of concentrated solar systems, applications for solar thermal industrial processes will become economically viable.

1.2 Objective

The heliostats represent 40-50% of the cost of a solar tower plant, so they must be relatively low cost for the cost of energy from the plant to be competitive with that of fossil fuels (Mancini et al., 2000). It was shown by Gary et al. (2011) that to achieve a levelised cost of electricity (LCOE) of 0.10 USD/kWh the heliostats must cost no more than 120 USD/m². The heliostats must cost about 75 USD/m² if the target LCOE is 0.06 USD/kWh (Gary et al., 2011). To achieve these targets, innovative designs and solutions regarding the complete heliostat concept and its components are needed. Furthermore, the dimensions of heliostats must be selected to minimize manufacturing and installation costs. This requires accurate estimation of the wind loading on both operating and parked (stowed) heliostats to allow structurally efficient heliostat designs to be developed with good optical performance characteristics, while avoiding structural failure. The objective of the presented thesis is to close knowledge gaps and to reduce uncertainties regarding the wind loading of heliostats.

Some of the main open questions regarding wind loads on heliostats were:

How can the wind loads on heliostats be reduced in an economic way?

Which is the optimum aspect ratio of the mirror panel?

At which heliostat field position do maximum wind loads occur?

Are the wind load coefficients of heliostats Reynolds number dependent?

Which turbulence properties have to be matched by wind tunnel tests?

Can the peak wind loads be reduced by shock absorbers? These open questions are addressed by the thesis.

1.3 Structure of the present study

At first, it is shown how the wind loads impact the heliostat design (2). Therefore, after a short description of heliostats (2.1) it is explained how the wind loads have to be taken into account for the dimensioning of heliostats (2.2) and how the wind loading can be reduced by the heliostat design or how the resistance of the heliostat against it can be increased (2.3).

Then it is investigated how heliostat properties impact the wind loading (3). An important property is the aspect ratio. For a wide range of aspect ratios, the wind load coefficients are determined by atmospheric boundary layer wind tunnel (BLWT) tests for varying elevation angle and wind direction. Reasons for the aspect ratio dependency of the different wind load components are given (3.1). Only few heliostat designs have wide gaps between mirror panels. Therefore, only one sample heliostat was measured to see whether wide gaps could have a significant impact on the wind loads (3.2).

Regarding heliostat fields (4), it is investigated how wind fences could reduce the wind loads at different positions (4.1) to address the question whether a wind fence is worthwhile. Peterka and Derickson (1992) measured an increase of maximum drag and lift within a field compared to an isolated heliostat but give no reasons for this increase. By BLWT tests, this thesis provides an explanation for this finding.

For realistic results of BLWT tests it is important to match certain wind properties (5). At conventional BLWTs the high Reynolds numbers associated with a storm cannot be reproduced at reduced scale. For heliostats in operation only negligible Reynolds number dependency is expected because the separation occurs at the edges of the heliostat. However, for stowpositionthe wind “sees” the round torque tube of the heliostat at which the separation points are not fixed and clearly defined. In a high-pressure wind tunnel with higher possible Reynolds numbers it was investigated whether this leads to a significant Reynolds number dependency of the wind load coefficients (5.1).

Besides the Reynolds number, it is important to match the turbulence characteristics of the flow. Turbulent energy spectra characterize the distribution of the turbulent energy over the frequencies of the fluctuations of the flow. Unfortunately, in conventional BLWTs the spectra cannot be fully matched because of the restrictions in size. It is investigated whether this mismatch has a significant impact on the measured wind load coefficients and pressure

distributions and whether the heliostat size and height is of impact on the wind load coefficients (5.2). The maximum gust duration causing the peak hinge moment in stow is measured by full scale measurements in (5.3). If short enough, load reduction could be achieved by shock absorbers. The background of the BLWT investigations is the theory of extreme value statistics and turbulent energy spectra.

2. Description of Heliostats

A good description of heliostats is given by Mancini (2000): “Heliostats provide the *fuel* for a power tower (sometimes referred to as a central receiver) power plant. Heliostats are named *helio* for sun and *stat* for the fact that the reflected solar image is maintained at a fixed position over the course of the day. They are nearly flat mirrors (some curvature is required to focus the sun’s image) that collect and concentrate the solar energy on a tower-mounted receiver located 100 to 1000 meter distant.”

The main heliostat sub-functions and their related components (Fig. 2) are the following (Pfahl, 2014):

Reflecting sunlight:	mirrors
Fixing mirror shape:	mirror support structure
Ground connection:	pylon and foundation
Offset determination:	control
Rotation of mirror panel:	drives



Fig.2 Heliostat Dimensioning Regarding Wind Loads

2.1 Heliostat Size

When the basic parameter of a heliostat, its size, is defined wind loads have to be taken into account. “What is the cost optimum size of a heliostat?” is a widely discussed but still open question. An analysis of the impact of the heliostat size on the cost is given by Kolb et al. (2007, Appendix A), showing that the curve of optimum size is quite flat. Therefore, the optimum size depends strongly on the specific conditions, and no general answer can be given. The main advantage of large heliostats is that less parts and fewer foundations are needed. The main advantage of small heliostats is that wind speeds are lower because of the low height and that their weight per mirror surface can be smaller. The reason for the lower specific weight is the following (Pfahl et al., 2017a):

By increasing the width and the height of the mirror panel the mirror area increases to the power of two. All other dimensions of the heliostat must be increased according to the width and height to avoid an increase of the stress caused by the peak wind loads. Therefore, the volume and the mass of the heliostat increase with increasing width and height to the power of three or with increasing mirror area to the power of 1.5 respectively (Kolb et al., 2007, A.3) (impact of larger wind loads due to larger wind speeds at increased height of larger heliostats neglected). Because the weight is a measure for the cost, especially for high production rates, small mirror support structures are advantageous due to their lower specific weight. Accordingly, for some heliostat concepts very small heliostat sizes were chosen (in particular, 2m² size in (Ricklin et al., 2014)).

However, also very large heliostats are realized (e.g. Titan-tracker) at comparably low weight and cost. The reason is that for larger heliostats more complex structures with low specific weight like frame work cantilever arms can be realized.

2.2 Tracking Accuracy

The tracking error is usually defined as the standard deviation of the difference between the actual and the ideal orientation of the optical axis of the heliostat across a year. Partly, the deviation can be caused by systematic errors like imperfect orientation of the rotation axes or errors in the calculation of the sun position. Systematic errors can be calibrated and corrected by aiming the focal spot to an extra target which is seen by a camera. The center of the focal spot is determined and the deviation from the given aim point is calculated.

This deviation is determined for several incident angles of the sun. With the deviations for different incident angles, the single errors can be calculated and corrected by the control (Berenguel, 2004).

The error caused by backlash of the drives cannot be corrected in this way. Backlash in combination with (turbulent) wind causes fluctuations of the position of the focal spot. If the drives are sufficiently pre-tensioned backlash has no impact at all. For the elevation axis, pre-tensioning can be realized by unbalancing the mirror panel. However, for the vertical axes, pre-tensioning by gravity is not possible. Fig. 3 shows a heliostat with pre-tensioning of the azimuth drive by spring elements. Usually, for the azimuth drive expensive high precision gears with low backlash are needed.

It is not trivial to calculate the standard deviation caused by a certain backlash because the influence of fluctuating wind conditions throughout the year and throughout the heliostat field and the breakaway torque have to be considered. Teufel et al. (2008) describe a method to calculate the impact of the



Fig. 3: Heliostat with pre-tensioned azimuth drive via spring (Brightsource Energy, 2012)

backlash on the annual energy yield of a plant. However, this method is yet to be validated. The standard deviation can be determined by measuring the deviation of the position of the centre of the focal spot for several characteristic periods of time to gain a probability distribution of the deviation. A Gaussian distribution can be fitted to it to achieve the standard deviation.

2.3 Deformation by Gravity and Wind during Operation

The heliostat structure must be rigid enough to avoid significant deformation due to changes of the mirror orientation. A deformation of the torque tube would lead to a misalignment of the mirror facets. Fig. 4 shows how the focal spot splits up for a heliostat with an under-designed torque tube. The facets are canted to achieve a small focal spot at solar noon. In early morning and late afternoon, the mirror panels and the torque tube are oriented differently which leads to a different deformation of the torque tube and a different angle of the facets relative to the torque tube, resulting in a significant slope error of the mirror panel.

Teufelet al. (2008) investigated the impact of gravity and wind loads on the annual energy yield. It was found that gravity can have a significant impact on optical losses, while wind during operation can usually be neglected. The reasons for the low impact of wind on the optical losses are the following: In operation, only the heliostats at the section of the field perimeter facing the wind (which is a very small portion of the total heliostat field) see significant wind loads while the others are in the wind shadow of the upwind heliostats.

The maximum loads occur only at certain angles of attack while for other combinations of wind direction and elevation angle the loads are much lower.

The maximum wind speeds for operation occur quite rarely.

When heliostats are attacked with significant wind speeds the focal spot will oscillate about a mean position. This will cause only small losses of energy while most of the energy will still hit the receiver. The reason is that the flux intensity is low at the edge of the focal spot. For vibrating heliostats near the tower it is possible no optical loss at all may occur, because their focal spot is small compared to the size of the receiver.

Heliostats must be designed rigid enough to be able to withstand storms in stow position and to have only low deformation due to gravity during operation. Hence, their deformation in the comparably low wind loads during operation is small.

Therefore, usually the impact of the wind loads on performance during operation can be neglected (for conventional heliostats with sufficient stiffness for all mirror orientations) which simplifies the design process significantly. However, the impact of wind loads on backlash during operation has to be taken into account (see section 2.2.2).

2.4 Survival during Operation and Storm

The peak wind load coefficients are lowest for the heliostat in stow position (i.e. a horizontal mirror panel) (Peterka and Derickson, 1992). However, these have to be combined with the highest wind speeds occurring during storms. Whether the different wind load components reach their highest values during operation or during storm in stow position depends on the maximum operational wind speed, the highest assumed storm wind speed and their corresponding wind load coefficients. As an example, the peak wind loads on a 30m² heliostat are calculated.

Wind and solar irradiation data (DNI) of Almeria, Spain, were analyzed to define the highest wind speed for which the heliostats still have to be in operation. At times with wind speeds below 10 m/s (at 10 m height) already about 97% of the solar energy is gained. Therefore, a limitation of the operational wind speed to 10 m/s is reasonable. The maximum wind speed that might occur while the heliostat moves into stow position is assumed to be 15 m/s (Ricklin et al., 2014, Table 1; Emes et al., 2015)). For the maximum wind speed usually the 50 year storm event is assumed (Cooke and Mayne, 1980). A typical value is a peak wind speed of $U_{peak} = 40$ m/s at 10 m height (NBE-AE-88, 1988, tab. 5.1), (DIN 1055-4, fig. A.1). with the wind load coefficients given by Peterka and Derickson (1992) the main peak wind load components for a heliostat with in a field were calculated. The mirror area is $A = 30$ m², chord length $h = 5$ m, elevation axis height $H = 2.9$ m, density of air $\rho = 1.25$ kg/m³ and gust factor $R = 1.6$. A vertical mean wind speed profile according to the power law with an exponent of $n = 0.15$ is assumed. The results are given in Table 1.

Table 1: Peak wind load components on 30m² heliostat (without safety factor) according to Peterka and Derickson (1992) including field factors

Wind load component	Max. $c_{peak, operation}$	Max.load operation	$c_{peak, stow}$	Load stow
Drag (F_x)	5.6	6.4 kN	0.6	4.9 kN
Lift (F_z)	3.8	4.3 kN	0.9	7.3 kN
Hinge moment (M_{H_y})	0.6	3.4 kNm	0.2	8.1 kNm
Moment pylon base (M_y)	6.2	20 kNm	1.0	23 kNm
Moment vertical axis (M_z)	0.7	4.0 kNm	0.02	0.8 kNm

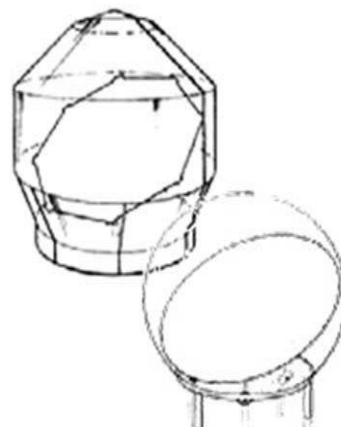
The drag force F_x and the moment about the vertical axis M_z reach their highest values during operation while the other wind load components are highest for stow conditions with high storm wind speed. For the dimensioning of heliostats the highest values of each wind load component have to be taken into account.

By strategic orientation of the mirror panels considering the wind conditions, the wind loads can be reduced with almost no additional cost. For example, the heliostat can be tilted about the elevation axis to a favorable orientation with respect to the wind direction during stow and storms (Gong et al., 2012) if the typical local weather conditions allow prediction of the wind direction. Alternatively, heliostats oriented in a position with a high wind load coefficient could go to stow position at lower wind speeds, or move to a slightly tilted orientation to protect other heliostats still in operation.

2.5 Wind Load Driven Heliostat Concepts

The highest loads on the structure occur at storm conditions. At these conditions the heliostats and PV-trackers are horizontally aligned to minimize the surface of wind attack (stow position). The wind loads can be further reduced or the resistance against them can be increased by the following heliostat design approaches (Pfahl, 2014).

Encased Solar Trackers



The most radical way to reduce wind loads and to protect the heliostats from sand and hail is to encase them by light-transmissive material, Fig. 5. Besides a reduced dimensioning this would enable the use of front surface mirrors with higher reflectivity. Drawbacks of the concept are the additional significant reflection at the encasement and the extra material for the light-transmissive material with its support structure



Fig. 4: Left: encased heliostats (Kolb et al., 2007), middle: inflatable heliostat (Sankrithi, 2012), right: parabolic trough in glass house (Glasspoint, 2015)

2.6 Lowering Mirror Panel during Stow

The loads on the mirror support structure could be reduced by lowering the mirror panel during stow at storm condition. For concepts with the elevation axis at ground level (Fig. 6, left column), the moment about the elevation axis at operation is higher than for conventional heliostats because the forces above and below the elevation axis are less balanced. For usual operational wind speeds, this higher hinge moment is in the same range or even higher than for conventional heliostats in stow position at storm. Furthermore, the moment is increased due to gravity. Therefore, lowering during stow would not lead to cheaper drive systems and also the cost for the mirror panels would not be reduced when the elevation drive is positioned and connected to the panel at its lower end.

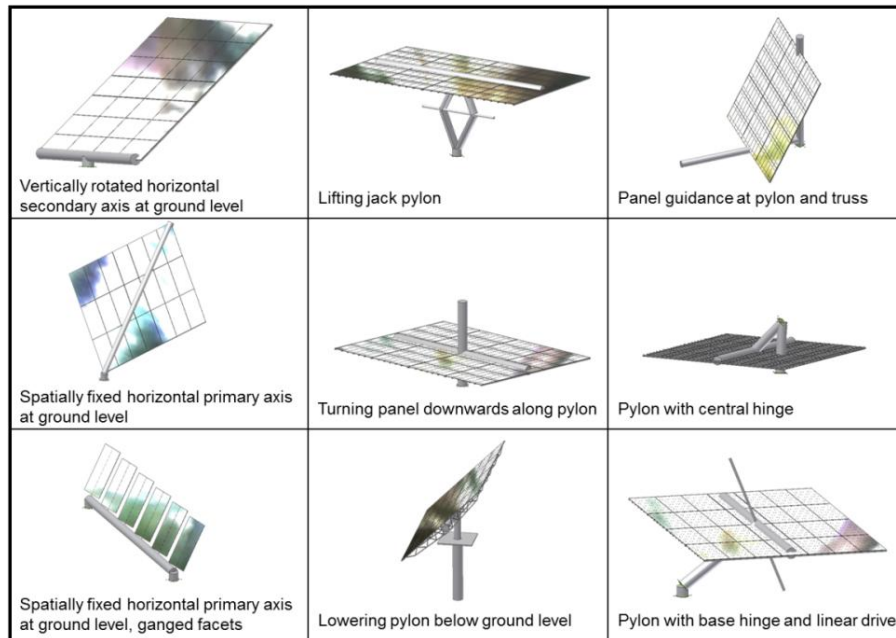


Fig. 5: Approaches for lowering mirror panel at storm condition (Pfahl, 2014)

However, if the elevation drive is connected to the centre of the panel (Fig. 7) low cost drives can be used and the maximum stress in the panel can be reduced by lowering it during stow. The higher moment about the elevation axis during operation due to gravity can be well handled by a spindle drive connected to the panel’s centre to achieve a long lever arm. This can be well realized in combination with a carousel carriage with wheel drive (Fig. 7).

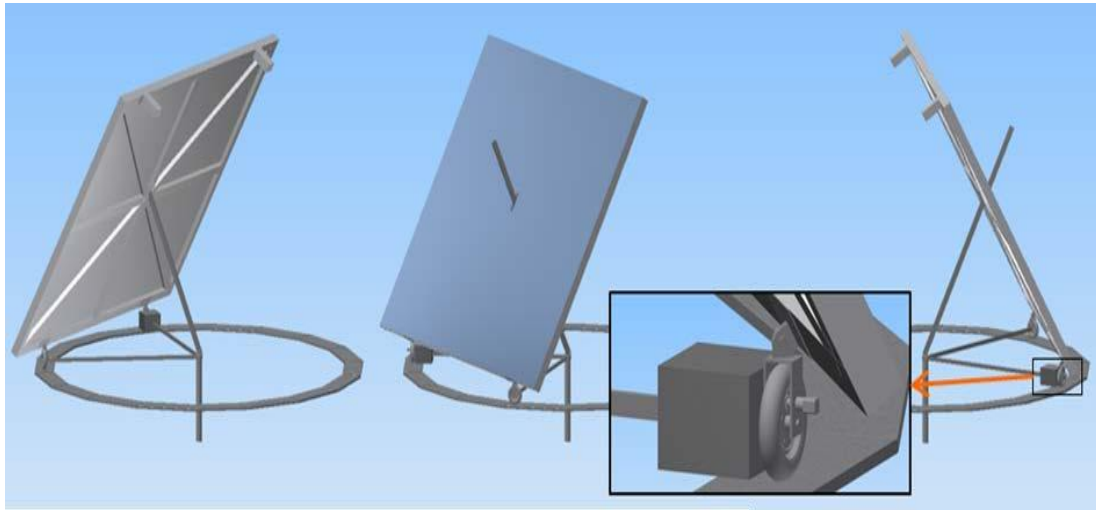


Fig. 6: Azimuthal rotation of a 50m² carousel type heliostat with wheel drive weighted against slippage (DLR) (Pfahl et al., 2017a)

For carousel type heliostats usually ring foundations are used on which the wheels are running to achieve high azimuthal accuracy (Deflandre et al., 1978; Mancini, 2000; Pérez-Rábago et al., 2012). However, such ring foundations are comparably extensive. A ring foundation could be avoided and the wheels of the azimuth drive could run directly on the ground or a simple pavement using a sensor that determines the orientation of the panel independently of the drive mechanism (Fig. 7) (Pfahl et al., 2015b). Such a sensor could be a camera chip with fish eye optics that detects the positions of the centre points of the sun and of the receiver at once. The centre point between these two recognised points is driven to the centre of the imaging space (Fig. 8, right). The normal of the mirror panel (N) is then centred between the vector to the sun (S) and the vector to the receiver (R) so that the rays from the sun hit the receiver (Fig. 8, left) (Pfahl et al., 2008).

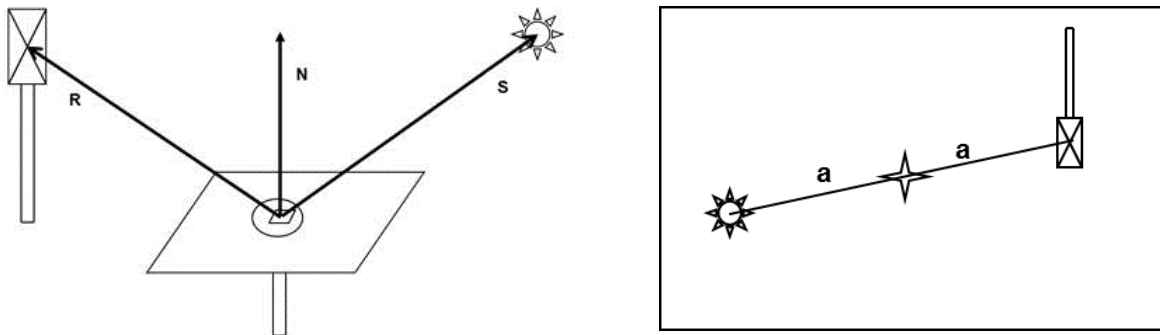


Fig. 7: Sun-target-sensor (Pfahl et al., 2008)

In addition with further innovations described in the following, a lowest heliostat cost of 75\$/m² (Pfahl et al., 2017a) is achievable (Pfahlet al., 2017b): The main component of the heliostat is a monolithic sandwich concentrator which combines the advantages of cantilever-arm and sandwich structures (Siegmeier, 2017). The concept avoids the complexity of canting using only one single facet. Thin glass mirrors sandwiched with a back structure yield high reflectivity and slope accuracy and hence increased optical efficiency. A simple carousel carriage with one actuated wheel realizes the azimuth movement. A low cost linear spindle actuator with the drive housed in the spindle passes through the panel's centre and induces the elevation movement. The heliostat uses a closed-loop optical sensor control. Therefore, the carousel carriage may run on a simple track of low accuracy requirements, which consists e.g. of compressed soil or concrete plates stuck together. The carriage is connected to the ground anchor which can be a pile driven into the ground. A weight of a concrete block or a sand-filled container on the actuated wheel avoids slippage during high wind loads. For stow, the spindle drive pulls the panel to the ground onto the wheels and two extra supports. Thus, the panel is well protected in storm. The reduced wind loads relax requirements and cost for the cantilever-sandwich concentrator (Fig. 9).

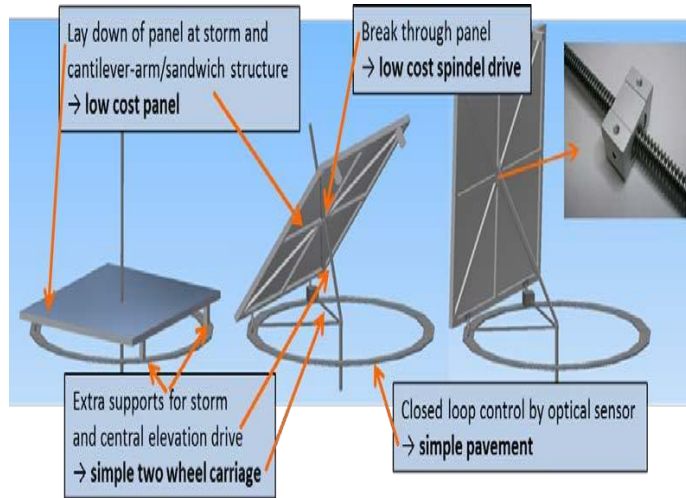


Fig. 8: Heliostat concept for minimum cost of all components (Pfahl et al., 2017b)

The disadvantages of the hitherto solutions, innovations, and resulting cost targets for producing 10 000 heliostats are listed for each part in Table 2.

Table 2: Set of innovations and estimated cost targets for 10 000 heliostats of 50 m² mirror area (Pfahl et al., 2017b)

Part	Disadvantage of hitherto solutions	Innovation (Patent)	Cost [\$/m ²]
Mirror panel	High wind loads	Lay-down for stow	29
	Many parts	Monolithic cantilever-sandwich panel (Siegmeier et al., 2017)	
	Expensive canting/mold	Low-cost large-size mold (Pfahl et al., 2016)	
Azimuth drive (carousel carriage)	Large, precise foundation ring	Simple pavement or compact ground sufficient due to closed loop control; ground anchor	12
	Extensive 4-wheel carriage	Low cost 2-wheel carriage sufficient due to central elevation drive and panel supports for stow	
	Expensive drive	Weighted wheel drive	
Elevation drive (spindle)	Telescope/scissor- mechanisms expensive	Direct spindle drive through central opening in panel	6
	Drive protection expensive	Drive housed in spindle (Ries, 2017)	
Control/ cabling	High accuracy of mechanical parts required	Closed loop control by optical sensor (Pfahl et al., 2008)	13
Fabrication/ installation/ profit			20
Total cost			80

2.7 Locking Device

For the stow position with its high possible storm wind loads the elevation drive can be unloaded by a locking device. Locking of the elevation can be easily realised using the azimuth drive as actuator (see Fig. 10: for locking the black bolt is positioned by the azimuth drive into the grey cramp). Locking of the azimuth drive is not needed because the loads about the azimuth axis in stow position are small.



Fig. 9: Locking of elevation drive during stow and framework facets, seen at Themis solar power plant heliostats.

Presumably, for conventional heliostats no cost reduction can be achieved by locking devices because for the elevation usually linear actuators are used: they are self-locking anyhow and the dimensioning of their spindles is not affected by an additional locking device because buckling is decisive for it which is small at stow position when the spindle is retracted. For drive concepts with increased lever arm like the rim drive concept (see section 2.3.4) locking could be realized at lower cost, because the locking device could use the lever arm of the drives.

Rim Drive Heliostats

The lever arm of the actuators is increased for heliostats with rims (Fig. 11) to reduce the torque on the drives and the accuracy requirements to be able to use low cost drives. The loads on the mirror support structure and partly on the bearings are reduced as well.

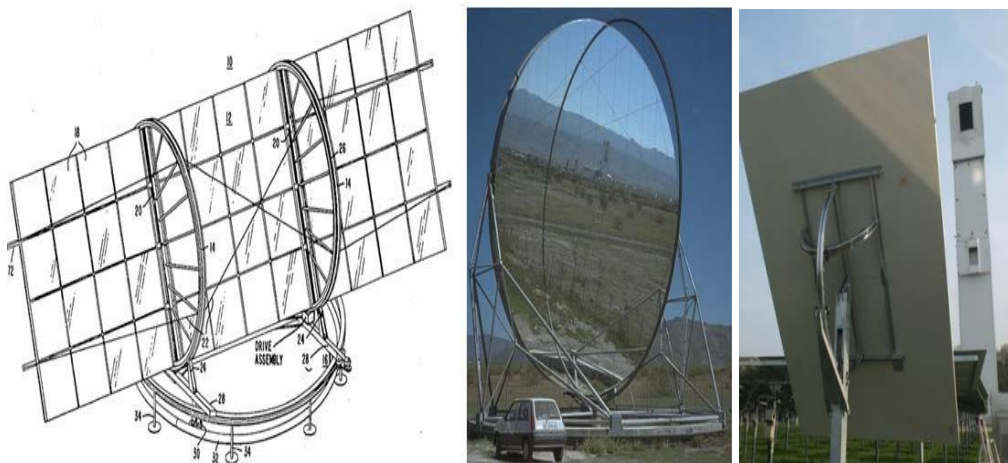


Fig. 10: Rim drive heliostats; left and middle: with vertical primary axis (Sayre, 1980; Weinrebe, 2000); right: with horizontal primary axis

For the rim drive heliostats with vertical (spatially fixed) primary axis shown in Fig. 11, left and middle, extensive foundation is needed. When the first axis is horizontal this can be avoided (Fig. 11, right) (Pfahl, 2011; Pfahl et al., 2013)). Drawback is that an extra guidance for the first rim is needed. By the rims the loads on the drives are reduced. Furthermore, the loads on the bearings, on the locking device (see section 2.3.3), on the mirror support structure, and on the upper part of the pylon (above the rim) are reduced (Fig. 12).

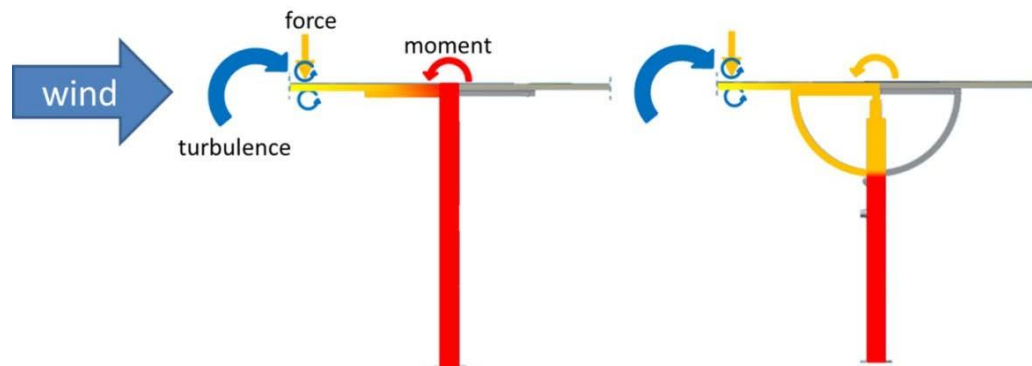


Fig. 11: The turbulence of the approach flow leads to a resulting force near the leading edge of the mirror panel causing a moment at the central bearing. By the rim this moment and thus the loads on drives, mirror support structure, locking device, central bearing, and upper part of the pylon are reduced. The colour change from yellow to red indicates increasing moment.

The rims can be driven via chains, traction sheaves or simply by winch wheels (Fig. 13). Winch wheels and chains (when pretensioned) have almost no backlash (Liedke et al., 2015).

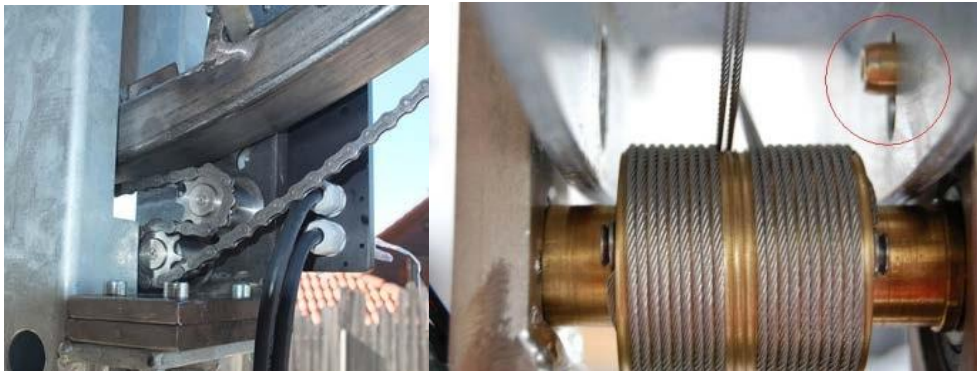


Fig. 12: Rim driven by chain (left) and by winch wheel (right) (with locking bolt (red circle))

The diameter of the sprockets of chain gears should be small to achieve a high gear ratio. Usually, small sprockets lead to fluctuating tension of the chain which reduces its lifetime (Liedke et al., 2015). However, by a special arrangement of the sprockets (Fig. 14, right) the fluctuating tension is avoided (Liedke et al., 2017).



Fig. 13: DLR 9m² rim drive heliostat with chain gear avoiding fluctuating tension of the chain caused by the polygon effect

Assuming e.g. a ten times longer lever arm for the drives, their torque capacity of the drives could be reduced by the same factor to one-tenth (Fig. 15).

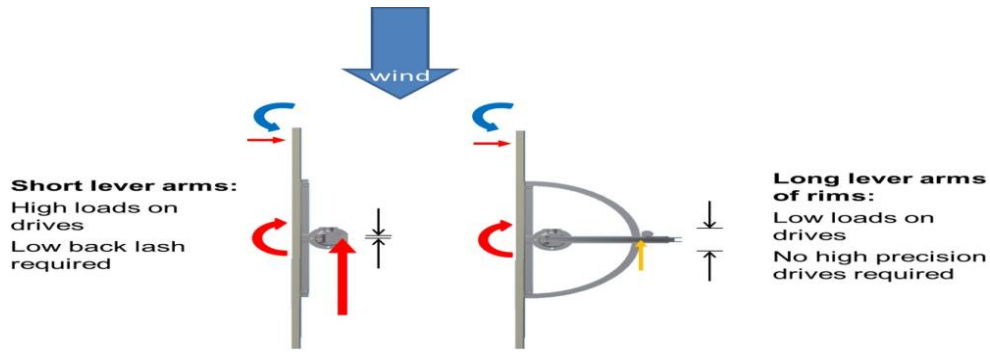


Fig. 14: Reduction of wind loads on drives and reduction of required precision of the drives by rims

A further advantage of the rims is the additional rigidity they provide, which leads to higher natural frequencies (4.7 Hz and 4.9 Hz for the first two modes, Fig. 16, left) and thus to lower dynamic loads (Liedke et al., 2017). The magnification of the hinge moment due to dynamic effects is only 1.4 (Fig. 16, right) compared to conventional structures with values in the range of 2 (Vásquez-Arango et al., 2015; Vásquez-Arango, 2016).



Fig. 15: Vibration behaviour of the heliostat structure at main modes (left and middle), time signals of input and output moment at the elevation axis with amplification factor 1.4 (right) (Vásquez-Arango, 2016)

For heliostats with horizontal primary axis the height of the elevation axis is increased by less than 20% compared to azimuth-elevation tracking because it is defined by the diagonal of the mirror panel and not only by the chord length. The increased height leads to somewhat increased wind loads compared to an azimuth-elevation heliostat of same area, especially at the pylon base (Pfahl et al., 2017a).

2.8 Spoilers

The wind loads on the mirror support structure could be reduced by spoilers mounted at the mirror panel (Peterka et al., 1986, Pfahl et al., 2014). Mainly the wind loads at storm are decisive for the dimensioning of the heliostat structure. Therefore, spoilers would have to be designed mainly for the stow position (horizontal mirror panel). Wind tunnel measurements showed a reduction of the hinge moment M_{Hy} of 40% (Pfahl et al., 2014).

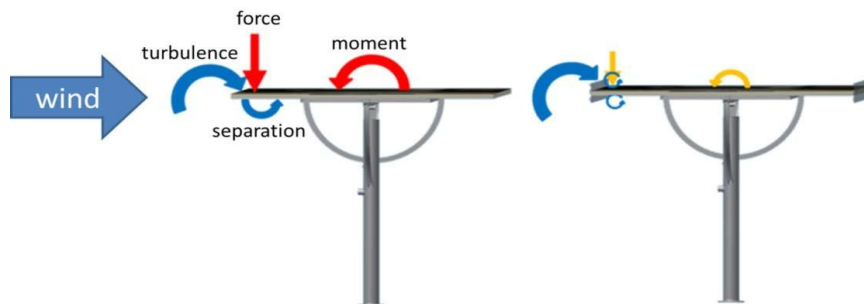


Fig. 16. Left: Turbulence of the approach flow causing separation at the frontal edge leading to high pressure coefficients c_p at the frontal edge and a high overturning moment. Right: Flow manipulators (fence like structures) reducing suction and overturning moment for heliostats in stow position

Without spoilers, the incident flow with vertical velocity component separates stronger at the frontal edge causing suction on the opposite side of the mirror. The resulting pressure difference between top and bottom of the facet leads to high pressure coefficients (cp-values) near the frontal edge (Pfahl et al., 2011a; Gong et al., 2013) and therefore to a high overturning moment, see Fig. 17, left. By a fence like structure at the frontal edge separation and thus suction is reduced, see Fig. 17, right.

3. Results and Discussion

F_x — horizontal force perpendicular to elevation axis(drag)

At load case 1 ($\alpha = 90^\circ, \beta = 0^\circ$) the heliostat is similar to a vertical flat plate with a gap of 0.4 m to the ground. For free standing plates on ground, the wind force coefficient decreases with increasing aspect ratio for aspect ratios < 5 (Sakamoto and Arie, 1983; Letchford and Holmes, 1994). (For slightly lifted plates this effect is reduced by only a small portion (ESDU 89050, figure 7c; Leder and Geropp, 1993). In the present study, an even more pronounced reduction of F_x for increasing aspect ratio was measured (Fig.25).

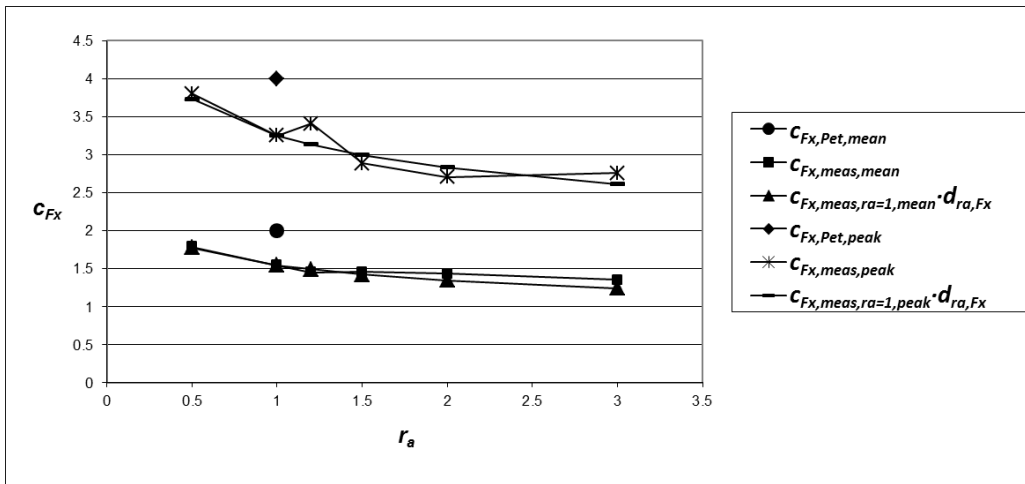


Fig. 17: Aspect ratio dependency of c_{F_x} at load case 1

For load cases 2 and 3 the projected mirror area is smaller than for load case 1 and therefore also the drag force. However, for high storm wind speeds and relatively low maximum wind speed for which the heliostat is in operation, the maximum drag force could occur during storms. At load case 4, the panel is horizontal ($\alpha = 0^\circ, \beta = 0^\circ$) in stow position which means that the cross bar is directly exposed to the wind. The cross bar increases with increasing aspect ratio as well as the frontal edge of the panel (Fig. 20, left). Therefore, F_x increases with increasing aspect ratio (Fig. 26). The calculated mean values are not in good agreement with the measured ones. The reason for it is not clear.

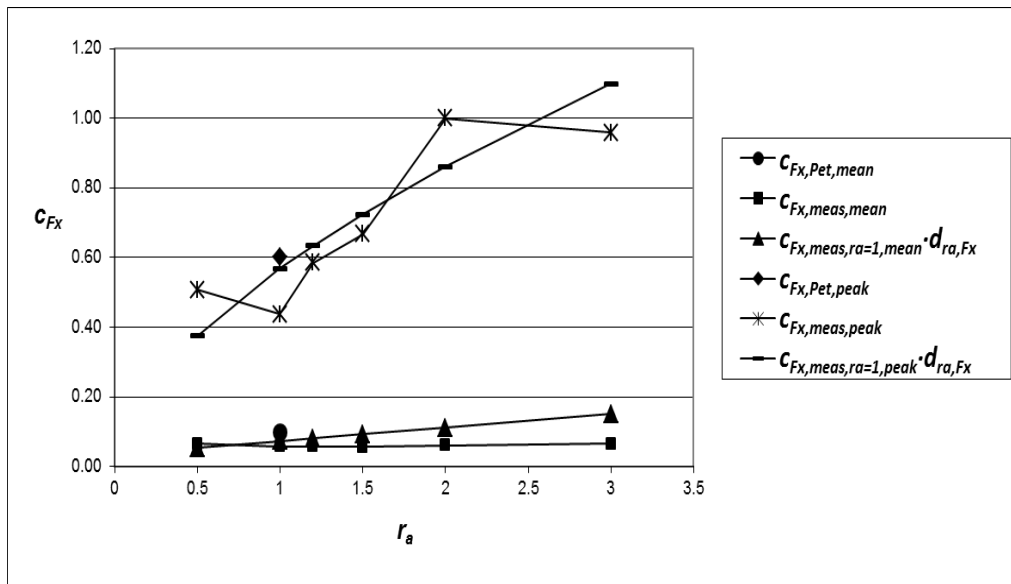


Fig. 18: Aspect ratio dependency of c_{F_x} at load case 4

F_y – horizontal force along elevation axis.

The values of F_y at load case 5 ($\alpha = 0^\circ, \beta = 90^\circ$) decrease (Fig. 27) because the area of attack (pylon and frontal edge of the panel) decrease with increasing aspect ratio (Fig. 20, right).

F_z – vertical force (lift).

The absolute values of F_z at load case 2 decrease slightly with increasing aspect ratio (Fig. 28). The reason might be that for bigger width b the gusts of maximal wind speed cover a smaller portion of the mirror panel.

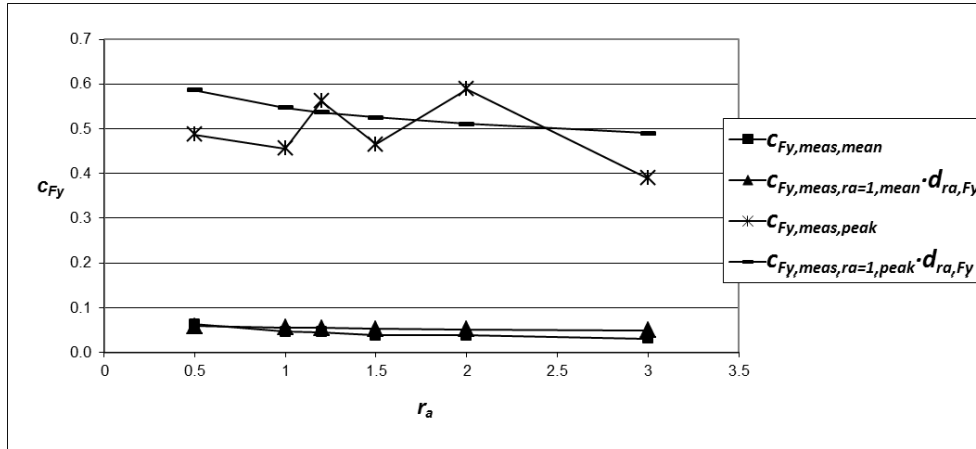


Fig. 20: Aspect ratio dependency of c_{Fz} at load case 2

For load case 4, the mean wind has no component normal to the mirror panel. Therefore, the mean values of F_z are very low (Fig. 29). The peak values are caused by turbulent gusts which lead to temporarily sideward wind attacks causing the high-pressure values at the frontal edge (Fig. 30, left). Since this edge increases with increasing aspect ratio, F_z increases as well. The high differences with the results from Peterka and Derickson (1992) particularly for this case are not clear.

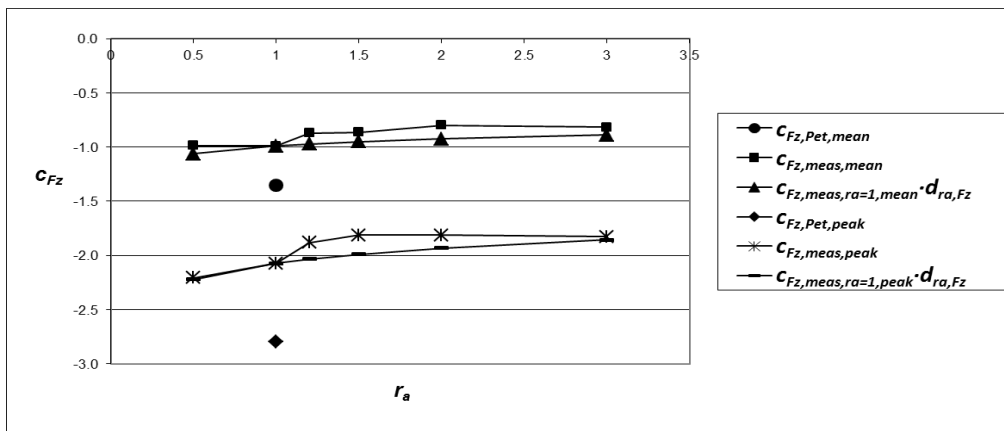
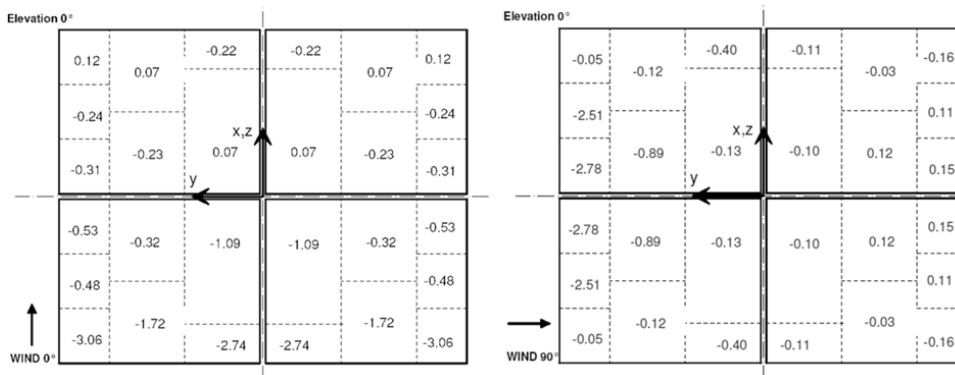


Fig. 21: Pressure coefficient distribution for aspect ratio 1.2 at point in time with peak F_z with $\alpha = 0^\circ$ and $\beta = 0^\circ$ (load case 4) (left) and peak M_x with $\alpha = 0^\circ$ and $\beta = 90^\circ$ (load case 5) (right).



M_x - moment at pylon base about x axis

Similar to F_z , the peak values of M_x are caused by a zone of high pressure at the frontal edge of the panel (Fig. 30, right). For the wind moments, this leads also to an almost constant aspect ratio dependency (which will be discussed in section 3.1.3.8) for load case 5 (Fig. 31). By Peterka and Derickson (1992) the definition of M_x is given but no values of the coefficient. Therefore, they are missing in the diagram.

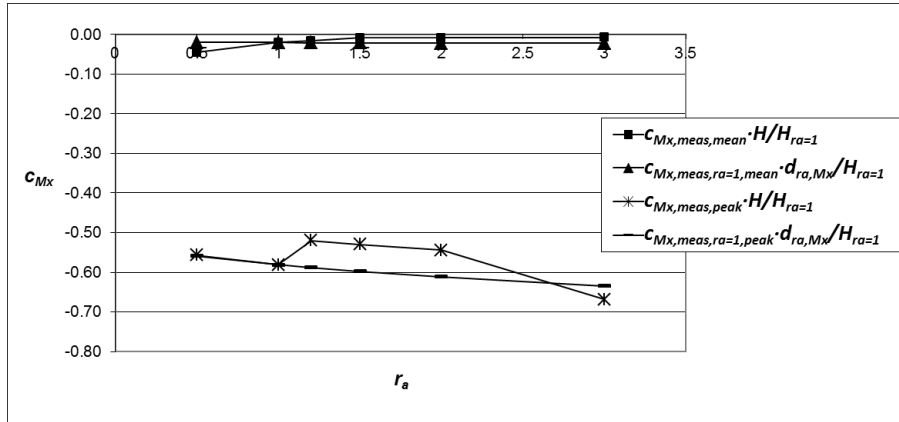


Fig. 22: Aspect ratio dependency of cM_x , normalised by the characteristic lever arm H for $r_a = 1$ at load case 5

M_{Hy} - hinge moment.

The definitions given by Peterka and Derickson (1992, p. 10) are assumed to be valid for all angles of attack and not to apply exclusively to special load cases. Furthermore, they are only valid for squared heliostats (p. 13). They did not intend to give aspect ratio dependencies of the wind load coefficients. However, for the wind moments an effective lever arm is accounted for according to equation (3.1.9). These lever arms are aspect ratio dependent and therefore an aspect ratio dependency is implicitly given by their formulas for the wind moments. For the hinge moment M_{Hy} , the effective lever arm (= characteristic length h) lead to a good agreement with the aspect ratio dependencies of this study (especially for load case 2, see Fig. 32) and are therefore given in the following diagrams.

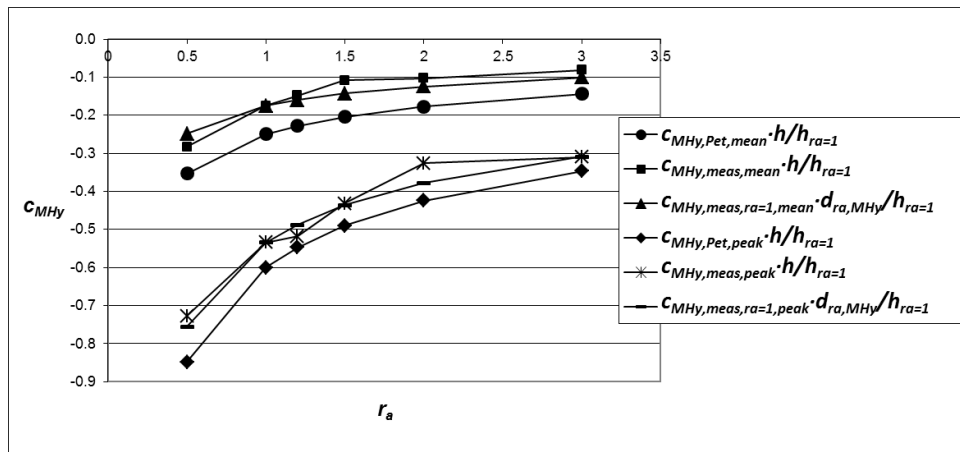
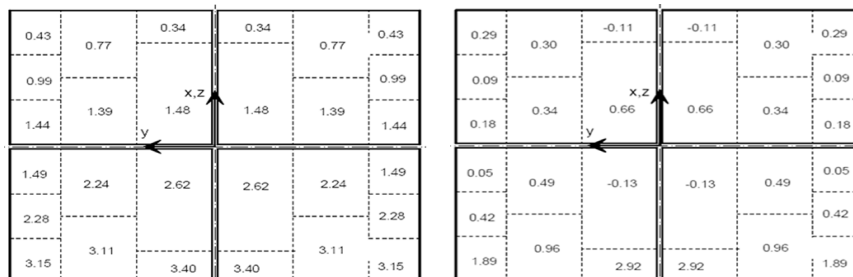


Fig. 23: Aspect ratio dependency of cM_{Hy} , normalised by the characteristic lever arm h for $r_a = 1$ at load case 2

The reason for this dependency is the almost linear pressure distribution at load case 2 (Fig. 33, left). For a linear pressure distribution, the lever arm of the resulting force is proportional to h whereas the value of the resulting force itself remains the same because the mirror area is not varied (this will be further discussed in section 3.1.3.8). Thus, all in all M_{Hy} is almost proportional to h .



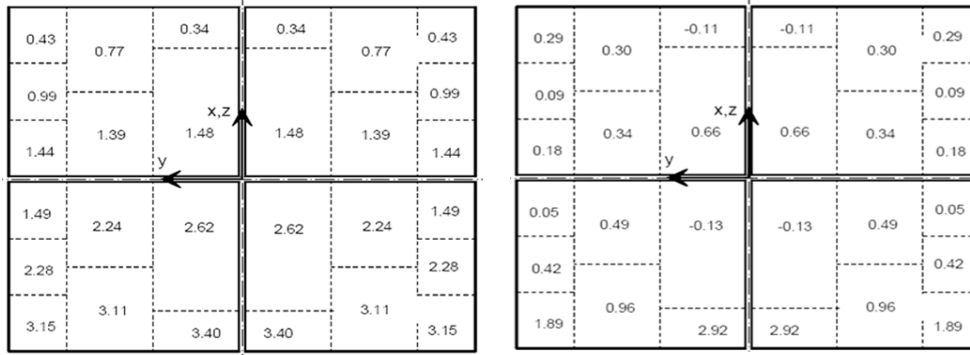


Fig. 24: Pressure coefficient distribution for aspect ratio 1.2 at point in time with peak M_{Hy} , with $\alpha = 30^\circ$ and $\beta = 0^\circ$ (load case 2) (left) and $\alpha = 0^\circ$ and $\beta = 0^\circ$ (load case 4) (right)

For load case 4 (Fig. 33, right) the pressure distribution which leads to the peak value of M_{Hy} is different to load case 2 (Fig. 33, left). At the frontal edge a small region of high pressure is measured. Presumably, it is caused by a turbulence structure which just hits the mirror panel there. The width of the frontal edge increases with increasing aspect ratio but the lever arm (distance of the frontal edge to the y axis) decreases (see Fig. 39). This explains why the aspect ratio dependency of M_{Hy} at load case 4 is less pronounced compared to Peterka and Derickson (1992, equation (4)) (Fig. 34) and to load case 2

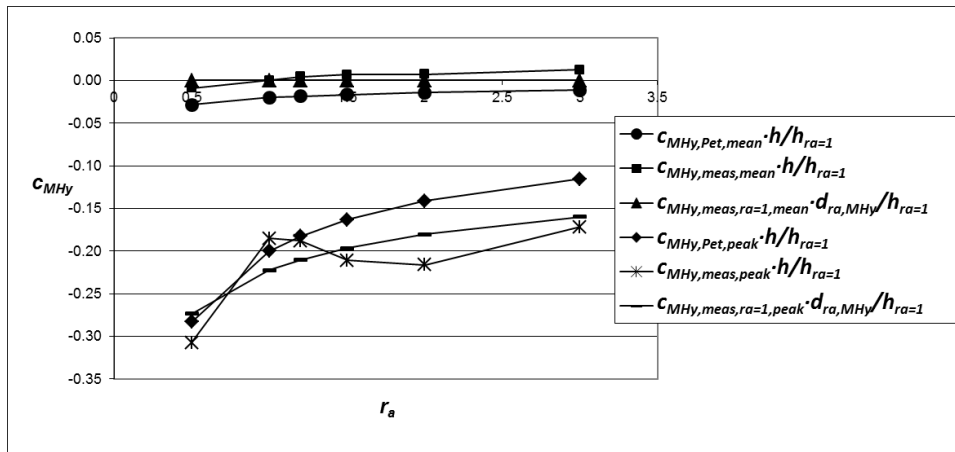


Fig. 25: Aspect ratio dependency of c_{MHy} normalised by the characteristic lever arm h for $r_a = 1$ at load case 4

M_y - moment at pylon base about yaxis.

Peterka and Derickson (1992, equation (6)) calculated M_y with

$$M_y = F_x \cdot H + M_{Hy} \quad (3.1.16)$$

At load case 1, M_{Hy} is relatively small so that equation (3.1.16) can be simplified to

$$M_y \approx F_x \cdot H \quad (3.1.17)$$

This explains the decrease of the load coefficient of M_y with increasing r_a (Fig. 35) for which H decreases.

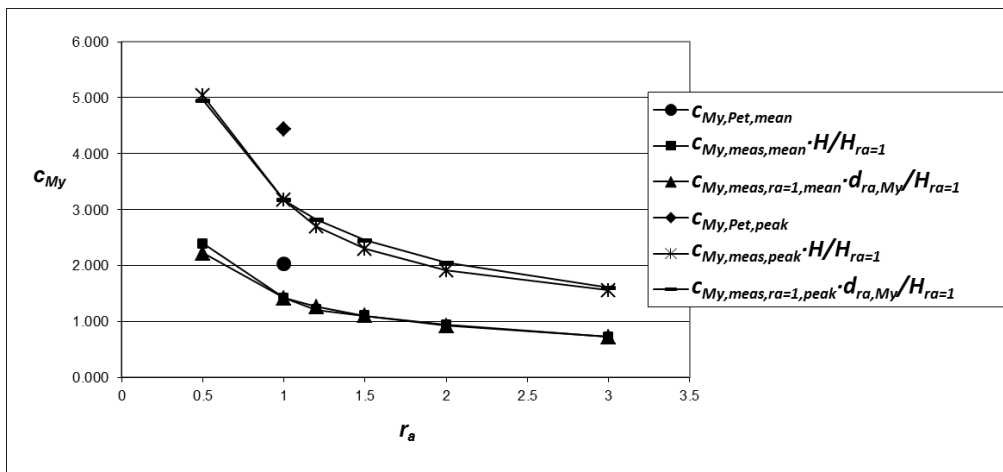


Fig. 26: Aspect ratio dependency of c_{My} normalised by the characteristic lever arm H for $r_a = 1$ at load case 1

For load case 4, M_{Hy} cannot be neglected. For this case, equation (3.1.16) leads to too high peak values of M_y , because the peak values of F_x and M_{Hy} do not occur at the same point in time since they are caused by different flow conditions. This partly explains the higher peak values of M_y of Peterka and Derickson (1992) at load case 4 (Fig. 36).

The values of M_y at load case 5 (Fig. 31) are lower than of M_y at load case 4 (Fig. 36) because of the orientation of the crossbar along with the wind direction which leads to a smaller area of wind attack.

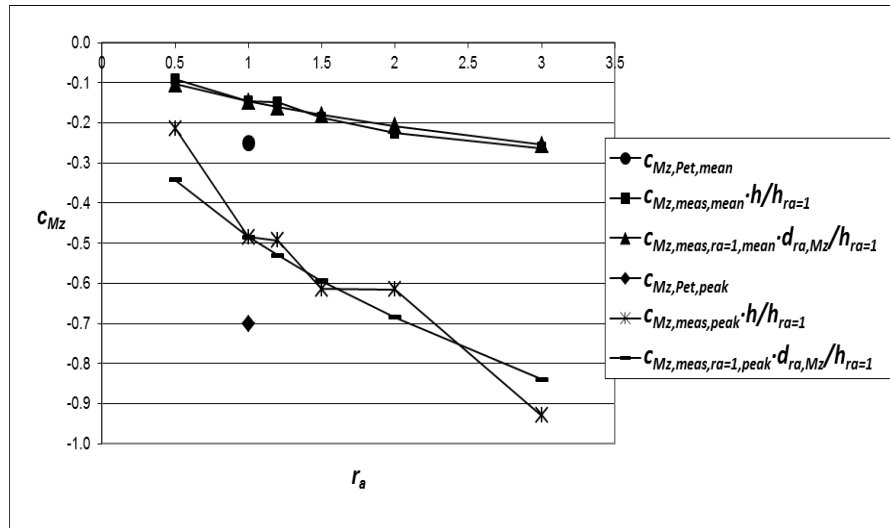


Fig. 27: Aspect ratio dependency of c_{Mz} , normalised by the characteristic lever arm H for $r_a=1$ at load case

4. Conclusions

Wide gaps in the mirror panel lead to an increase of the pressure distribution at the edges of the gap, especially at the windward corners. This causes an increase of the hinge moment of about 20% for an angle of attack of 30° to the panel and for a main flow direction along the gap. The peak hinge moment at stow position is also increased by this effect because it is caused by an instantaneous sideward angle of wind attack.

REFERENCES

- [1] Cook, N.J., Mayne, J.R., 1980. A refined working approach to the assessment of wind loads for equivalent static design. Journal of Wind Engineering and Industrial Aerodynamics, 6, 125-137. ESDU 89050, 1990.
- [2] Boundary walls, fences and boardings: mean and peak wind loads and overturning moments. Engineering Science Data, Wind Engineering Series, 2b, London. Fröhlich, J., 2006. Large Eddy Simulation turbulenter Strömungen, Teubner, Wiesbaden. Hucho, W.H., 2002.
- [3] Aerodynamik der stumpfen Körper, Braunschweig/Wiesbaden. Leder, A., Geropp, D., 1993. Analysis of unsteady flow past bluff bodies. Journal of Wind Engineering and industrial aerodynamics, 49, 329-338.
- [4] Letchford, C.W., Holmes, J.D., 1994. Wind loads on free standing walls in turbulent boundary layers. Journal of Wind Engineering and Industrial Aerodynamics, 51, 1-27. Mathey, F., Cokljat, D., Bertoglio, J.P., Sergent, E., 2006.
- [5] Assessment of the vortex method for Large Eddy Simulation inlet conditions. Progress in Computational Fluid Dynamics, 6, 58-67. Peterka, J.A., Derickson R.G., 1992. Wind load design methods for ground based heliostats and parabolic dish collectors. Report SAND92-7009,
- [6] Sandia National Laboratories, Springfield. Peterka, J.A., Hosoya, N., Bienkiewicz, B., Cermak, J.E., 1986. Wind load reduction for heliostats, Report SERI/STR-253-2859, Solar Energy Research Institut, Golden, Colorado. Peterka, J.A., Tan, Z., Cermak, J.E., Bienkiewicz, B., 1989.
- [7] Mean and Peak Wind Loads on Heliostats. Journal of Solar Energy Engineering, 111, 158-164. Plate, E.J., 1982. Wind tunnel modeling of wind effects in engineering, in: Plate, E.J. (Ed.), Engineering Meteorology, Studies in Wind Engineering and Industrial Aerodynamics, 1, Else vier, Amsterdam – Oxford – New York, pp. 573-639.
- [8] Sakamoto, H., Arie, M., 1983. Flow around a normal plate of finite width immersed in a turbulent boundary layer. Trans ASME, Journal of Fluids Engineering, 105, 98-104. Sergent, E., 2002. Versune Méthodologie de Couplage entre la Simulation des Grandes Echelles et les Modèles Statistiques, PhD

Thesis, L'EcoleCentrale de Lyon. 30 Spalart, P.R., 2000.

- [9] Strategies for turbulence modelling and simulations. *International Journal of Heat and Fluid Flow*, 21, 252-263. Wang Y.G., Li, Z.N., Gong, B., Li, Q.S., 2008. Wind Pressure and Wind-induced Vibration of Heliostat, *Key Engineering Materials*, 400-402, 935-940. Wu, Z., Wang, Z., 2008. Numerical study of wind loads on heliostat. *Progress in Computational Fluid Dynamics*, 8, 503-509. Wu, Z., Gong, B., Wang, Z., Li, Z., Zang, C., 2010. An experimental and numerical study of the gap effect on wind load on heliostat, *Renewable Energy*, 35, 797-806.